Journal of Student Scholarship

Volume 1
Issue 1 *Special Issue (June-July 2020)*

Article 4

2020

Laboratory Plasma Tests Towards the Production of Simulated Supernova Shock Waves

Elatia Zaffke
St. Cloud State University, eazaffke@stcloudstate.edu

John Sinko
St. Cloud State University, jesinko@stcloudstate.edu

Matthew Thomas
St. Cloud State University, matt_jthomas@live.com

Elisha Polomski
College of San Mateo, epolomsk@gmail.com

MINNESOTA UNDERGRADUATE SCHOLARS

Proceedings of the 9th Annual Minnesota State Conference of Undergraduate Scholarly and Creative Activity
and
St. Cloud State University Journal of Student Scholarship, Vol. 1, Special Issue 1, 2020

MINNESOTA STATE

Laboratory Plasma Tests towards the Production of Simulated Supernova Shock Waves

Elatia A. Zaffke[1], John E. Sinko[1], Matthew Thomas[1], and Elisha Polomski[2]

[1]*Department of Physics and Astronomy, St. Cloud State University, St. Cloud, MN*
[2]*Department of Astronomy, College of San Mateo, San Mateo, CA*

Abstract

Supernovae are some of the most powerful explosions that occur in our universe. These explosions generate massive shock waves that span tens of light years in distance. They are responsible for atomic fusion that creates the denser elements, needed for the creation of planets such as our own. The goal of this project was to simulate a supernova on a small scale, in order to study the resultant shock waves and their effects upon the interstellar medium. This research can improve understanding of the impact these events have upon the formation of solar systems and the composition of the interstellar medium itself. In order to simulate a supernova in the lab, two electrodes were fashioned from sputter-coated aluminum and affixed within a scientific vacuum chamber. The vacuum chamber was pumped down, then re-pressurized with helium or argon gas. A 13.56 MHz radio frequency plasma was sparked and maintained using a 120-Watt RF generator and matching network. Characteristic UV-Vis-NIR spectra for argon and helium were recorded as functions of pressure, power, and position in the chamber. An attempt was made to capture high speed images of shock waves during vaporization of a graphite rod in the plasma chamber, but was ultimately unsuccessful.

Introduction

Supernovae are phenomenally energetic events resulting from the death of a high mass star, or the nuclear detonation and complete destruction of a white dwarf within a binary system. The energy released in the well-studied Supernova 1987A was more than 10^{46} Joules; equivalent to the simultaneous explosion of about 10^{32} atomic bombs. Many elements are made by the process of nuclear fusion in the core of a star. As a star reaches the end of its lifetime its mass begins to flows into the core. When the star has exhausted its nuclear fuel and can no longer withstand its own gravitational force, the core collapses and results in a supernova explosion. This explosion sends shock waves outward into interstellar space, carrying heavier elements and debris with them. These elements take part in the formation of new stars, planets and more. By simulating these supernovae, albeit on a much smaller scale in the laboratory and well below the pressure and temperature required for nuclear fusion, we can nevertheless study how the shock waves travel through and impact the interstellar medium.

These cosmic explosions link both the death and birth of stars and planets.[1] A shock wave from a supernova explosion likely initiated the collapse of the cloud of gas and dust from which our Sun and the

Earth formed.[2] Based on this idea, shock waves can also change the chemical characteristics and morphology of dust that they encounter and seed it with trace elements.

Although the attempt to mimic a supernova at the laboratory scale may seem a bit limiting, the results can still explain observations on a much grander scale. During a supernova, large fluxes of high energy particles are emitted with energies dependent on the supernova shock wave itself. The finite lifetime and the curvature of the shock front are determining factors on the maximum allowable energy of emitted cosmic rays. The effects of these shock waves also affect the observations of interstellar space, where turbulence caused by supernova shocks can cause fluctuations in observed spectra.[3] Energy deposition, shock expansion rate, and the duration of the supernova event also have a large effect on the flow of matter within the supernova event. This flow of matter is profoundly important for astronomical observations long after the event has taken place. Large inhomogeneities in the expanding shell of debris from a supernova event are the result of this flow of matter and determine the composition of stars and planets that form from the material long after it has been ejected.[4] The heavy element abundances in the subsequent generation of stars can be used to determine the age of stellar bodies and how many generations of supernova events preceded their formation. The traces of past supernova events can even be seen in isotropic anomalies in meteorites within our own Solar System [2] Our work with RF discharge plasmas in a laboratory environment will provide key insight to what happens inside of a supernova event.

Radio frequency (RF) glow discharge plasmas have found frequent use in industrial and scientific lab environments due to their stability and utility. In an RF capacitive coupled plasma (CCP), an RF generator (AC in the diagram) delivers electromagnetic power to a load. [5] In our case, the load is a plasma tuned by a matching network MN, portrayed conceptually in Figure 1.

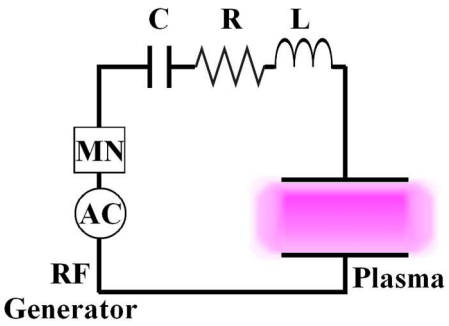

Figure 1: Conceptual Electrical Diagram for a Capacitive RF Plasma

The system is characterized by values of resistance R, inductance L, and capacitance C, which are endemic to the components (wiring, connectors, vacuum chamber), as well as to the state of the plasma and RF generator output. Tuning of impedance via capacitive adjustment within the matching network maximizes power delivery to and absorption by the plasma.

When a plasma is ignited from a gas, a significant number of gas particles are ionized. A plasma is quasi-neutral, meaning its composition includes roughly equal numbers of positive and negative charges. The plasma shields electrical information to about one Debye length, given by:

$$\Lambda_D = \sqrt{\frac{e_0 k_B T_e}{n e_c^2}}, \qquad (1)$$

where e_0 is the dielectric permittivity of free space, k_B is the Boltzman constant, T_e is the electron temperature, n is particle number density, and e_c is the electric charge constant [6(a)].

The mean free path of a particle in a gas describes the average distance the particle travels before colliding with another particle. Its value is given by [6(b),7]:

$$\Lambda = \frac{1}{n\sigma} = \frac{k_B T}{p\frac{\pi}{4}(d_1^2 + d_2^2)}, \qquad (2)$$

where σ is the collision cross section, T is thermal temperature, p is pressure, and d_1 and d_2 are the effective diameters of the particles participating in the collision, under the assumption of spherical particles. This path length can influence the behavior of a plasma in a scientific vacuum chamber, in particular, determining whether the gas particles collide more with the wall (molecular flow) or with each other (collisional flow).

According to the Schrödinger equation, electrons in an atom can only exist at discrete energy states within an atom, which are dependent upon a set of quantum numbers [6]. These numbers include n (energy quantum number), m_l (magnetic quantum number), l (orbital angular momentum quantum number) and s (spin quantum number). A set of rules governs these fundamental quantum numbers, which are expressed in Table 1:

Table 1: Basic Rules Governing Quantum Numbers

Quantum number	Description	Allowed values
n	Energy	1, 2, 3, …
l	Orbital Angular Momentum	0, 1, …, n-1
m_l	Magnetic	-l, -l+1, …, l-1, l
s	Spin	-½, ½

In chemistry, values of l are assigned letters (s,p,d,…) that designate "subshells," e.g., l = 0 (s), l = 1 (p), and l = 2 (d). These can be structured to express the electronic state of an atom; for example, atomic helium with 2 protons, has 2 electrons in the 1st shell, would have electronic state $1s^2$. Argon, with 18 protons, has complete electronic state: $1s^2 2s^2 2p^6 3s^2 3p^6$. Collisions with particles and exchange of photons can result in transitions of electrons between states, including those at higher energies.

Ionization energies are the energy values necessary to completely remove an electron from an atom or ion. These are important in setting threshold behaviors for plasma, and values for Argon and Helium are organized in Table 2 [9]:

Table 2: Ionization Energies of Argon and Helium [9]

	Units	Argon	Helium
1st Ionization Energy	eV	15.7596117	24.58738880
2nd Ionization Energy	eV	27.62967	54.4177650

Argon is characterized by a significantly lower energy first threshold to ionization compared to helium, and thus might be expected to be easier to ignite as a plasma. The values are stated to significant digits matching the precision currently accepted by NIST.

An electron moving from a higher energy state to a lower state within an atom or ion emits a photon with a precisely defined energy. Since frequency and energy of a photon are proportional, these photons have frequency values that are fundamentally determined by the set of quantum numbers of the source. This is the basis for optical spectroscopy. A characteristic and unique set of energy levels and emission lines exists for each element. We can use these emission lines to identify constituents of the plasma. The ten strongest spectral lines of argon and helium from 300-1000nm wavelength are collected in Table 3(a) and Table 3(b). [9]

Some past literature work also addressed spectroscopy of helium and argon plasmas.[10] Some studies included the practical step of calculating plasma temperature from spectroscopic data.[11] We have not yet completed this analysis on our own data as of the writing of the present work.

Table 3(a): Strong Lines of (a) Argon [9]

Argon		
Wavelength [nm]	Intensity	Attribution
750.4	600	Ar I*
763.5	700	Ar I
794.8	600	Ar I
800.6	600	Ar I*
801.5	700	Ar I
810.4	600	Ar I*
811.5	1000	Ar I*
842.5	600	Ar I*
912.3	1000	Ar I*
965.8	700	Ar I

Table 3(b): Strong Lines of Helium [9]

Helium		
Wavelength [nm]	Intensity	Attribution
301.4	40	He I
388.9	500	He I*
402.6	50	He I
447.1	200	He I
471.3	34	He I
501.6	100	He I*
587.6	870	He I*
667.8	200	He I*
706.5	180	He I*
728.1	50	He I

*These lines had the strongest intensity in our experimental observations

Other past efforts simulated a supernova explosion in the laboratory, include a simulation of the collision of shock waves with ring nebula material.[12]

One major objective of this set of experiments was to ignite a laser-driven detonation wave, or shock wave, within the plasma. To achieve such a detonation requires extremely concentrated energy per volume within a material. To produce such concentration with a laser in turn requires significant energy to be forced into a tiny space. The smallest achievable laser spot diameter is called the diffraction limited spot diameter, d, and it is given for a focused, Gaussian, stigmatic laser beam by:

$$d = \frac{2.44\, f\, \lambda}{D} \qquad (3)$$

where f is the focal length of the lens, λ is the laser wavelength, and D is the effective beam diameter focused onto the target by the lens [13].

Next, we will present the experimental equipment and methods used in this study.

Experiment and Methods

For the main experiment setup shown in Figure 2, two electrodes were fashioned from 6061 aluminum and each was plasma sputter coated (Quorum, SC7620) with gold-palladium alloy for 60 seconds on one face. Each electrode was held within a separately fashioned polyvinyl chloride insulating shield and supported by polycarbonate rods, then affixed within a scientific vacuum chamber of approximate volume 0.003 m^3. The vacuum chamber was pumped down to approximately 0.8 Pa using a rotary vane pump (Ulvac Kiko, GLD136C).

Following evacuation, the chamber was re-pressurized with a test gas (argon or helium) to a specified pressure within a chosen range from 5-270 Pa, measured with a Pirani gauge (Kurt J. Lesker, 275i). A 13.56 MHz, 120-Watt radio frequency (RF) generator (T&C Power, AG 0113) and matching network (T&C Power, AIT-600-03) sparked and maintained a glow discharge RF plasma for the experiments. Plasma voltage and RF power reflection was monitored by the matching network.

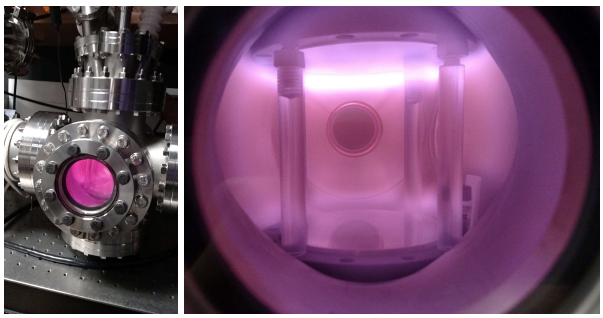

Figure 2: General Experiment Setup

For all parts of the experiments, plasma spectroscopy was performed using a UV-Vis-NIR spectrometer (Ocean Optics, Flame) using the setup shown in Figure 3, with irises and collimating optics used to restrict the field of view to a column within the plasma of about 1 cm diameter.

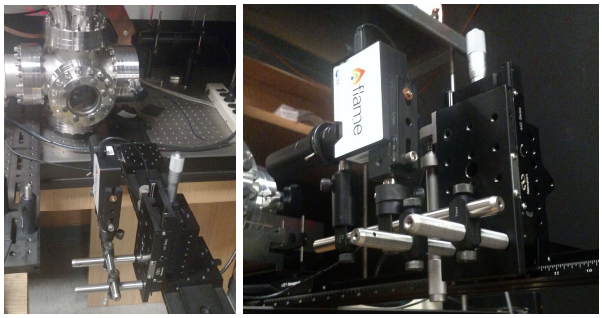

Figure 3: Spectroscopy Experiment Setup

For the power tests, the power delivered to the plasma was incremented using the RF generator and matching network including specific settings at 1 W and 2 W, and incremental steps of power from 5-100 W using intervals of 5 W. A dark spectrum (room lights and plasma off) was subtracted from each measurement. An integration time of 100 ms was used, with each spectrum comprising an average of 11 scans, with spectral binning using a size 3 boxcar window.

For the laser ignition tests, a pulsed Nd:YAG laser (Continuum, YG-660) delivered 1064nm wavelength, 0.1 J per pulse into the plasma by directing the beam from a series of mirrors and finally into the vacuum chamber through a lens. For a secondary part of this effort, a graphite rod was inserted into the chamber at the focus of the laser beam and ablated.

Results

The experimental results are divided between three main areas: first, a test of dependence upon power, a second test probing the spatial distribution of temperature in the plasma, and third, a test to attempt to ignite the plasma using laser energy deposition. Finally, we will report details of an unsuccessful attempt to capture images of shock waves during vaporization of a graphite rod.

MINNESOTA UNDERGRADUATE SCHOLARS
Proceedings of the 9th Annual Minnesota State Conference of Undergraduate Scholarly and Creative Activity
and
St. Cloud State University Journal of Student Scholarship, Vol. 1, Special Issue 1, 2020
MINNESOTA STATE

I. Power Tests

In this series of tests, argon or helium was added to the chamber continuously with the roughing pump running, to maintain the pressure at 80. ± 1 Pa. Meanwhile, the RF forward power to chamber was adjusted from 1-100. W. At each power setting (1 W, 2 W, and 5-100. W in 5 W intervals), the plasma voltage was noted and a set of three UV-Vis-NIR spectra recorded. Whereas helium plasma was produced across the entire range of power settings, argon could only be ignited above 2 W. This lower limit in power to produce an argon plasma was observed in other plasma physics studies and was attributed to argon exhibiting higher resistance than helium.[7] Three-measurement averages for plasma voltage are shown as a function of power in Figure 4.

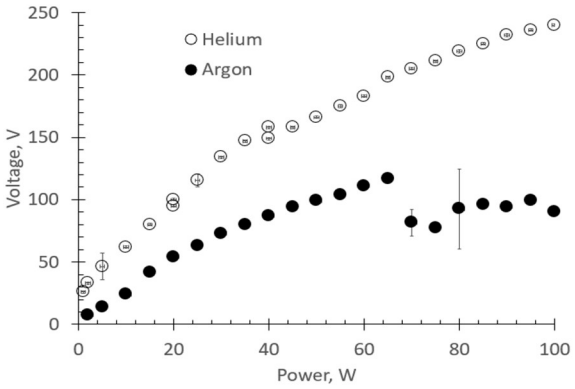

Figure 4: Plasma voltage as a function of RF power

Following the ignition of plasma, spectra of RF-sustained helium and argon plasmas were measured by UV-Vis-NIR spectroscopy. The line spectra of the two gases are of course distinct. The measurements are presented in Figure 5.

Noting the broader peaks common to both plots, there is clearly a significant background, which we believe may arise from one or more of four possible sources: (1) hydrogen and/or oil contamination in the chamber from the rough vacuum pump, (2) chlorine outgassing from the PVC insulating shields, (3) air (nitrogen/oxygen) leak in the gas line, or (4) sputtering of aluminum from the electrodes. Regardless of the source of the background features, each spectrum includes several lines that are clearly present for one gas and not the other, and these generally align with expected strong lines of argon or helium.

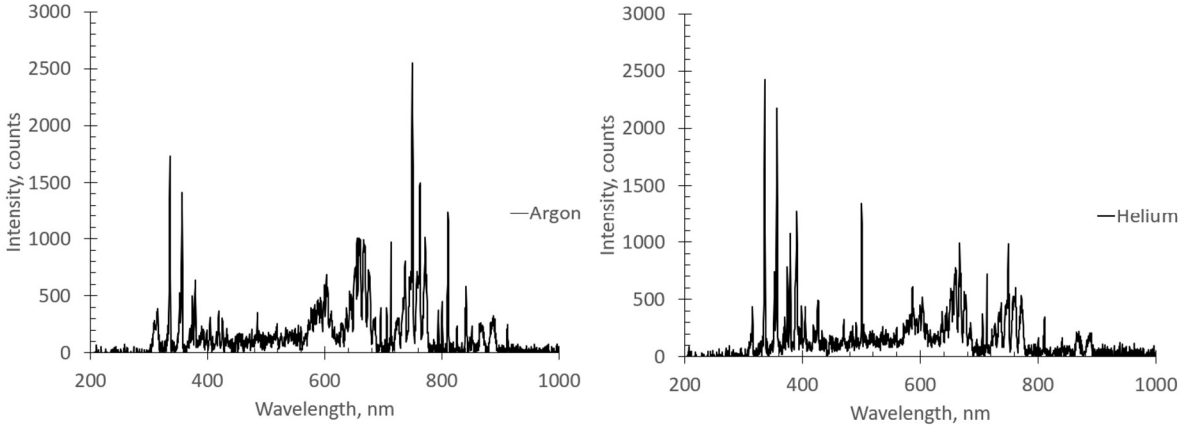

(a) (b)

Figure 5: Experimental (a) argon and (b) helium spectra

For helium, the 501 nm line was particularly visible, and deemed to be of analytical importance. Its intensity dependence upon power is illustrated in Figure 6(a).

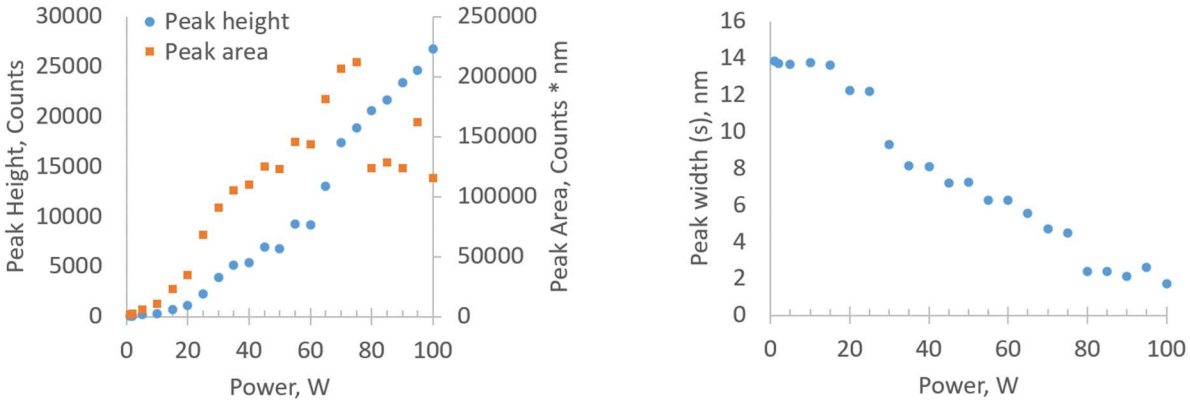

(a) (b)

Figure 6: Helium 501nm line spectral output with power: (a) Peak height and area, (b) Peak width

As demonstrated in Fig. 6(a), the data seem to evince a power law increase in peak height up to about 75 W, which was followed by an approximately linear increase to 100 W. Over the entire range, peak width decreases approximately linearly with increasing RF power, as shown in Fig. 6(b).

II. Pressure Tests

In this series of experiments, the pressure in the chamber was varied from 5-270 Pa for argon or helium flowing through the system, with a constant forward power setting of 20. W, and with the vacuum pump running. At each pressure, plasma voltage was recorded, and three UV-Vis-NIR spectra were collected and averaged. Results are shown in Figure 7(a) for argon and 7(b) for helium.

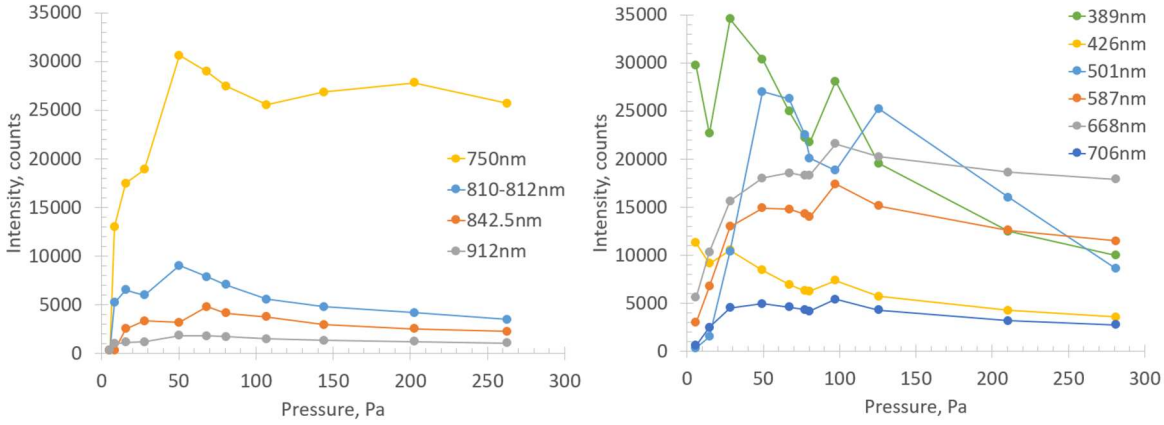

(a) (b)

Figure 7: Spectral intensity of strong lines with increasing pressure: (a) argon, (b) helium. The lines connecting data points are for clarity in identification, and are not intended to indicate trend lines.

In general, the intensity of the lines in both plots rapidly rises as pressure increases from our system baseline of around 40 mTorr (5 Pa) up to a few hundred mTorr, then slowly falls off as the pressure is further increased. It may be noted that our RF device failed to ignite argon above 2 Torr (270 Pa). This is likely due to collisional interference in the RF electron acceleration mechanism, in conjunction with decreasing mean free path as pressure increases. The interesting exceptions to the general behavior are the

357nm and 389nm lines for helium, which seemed only to decrease in intensity with increasing pressure. The existence of the observed helium lines points to significant population of various energy states around 23 eV, which it may be noted is quite close to the ionization energy for helium.

III. Vertical Translation Test

In this experiment, the vertical position of the UV-Vis-NIR spectrometer was adjusted in steps of 11 mm. The spectrometer input was carefully tuned using a set of irises and lenses to permit entry of light from a region of only around 11 mm diameter. This repositioning allowed creation of a vertical map of spectral output within the plasma by taking successive vertical steps of 11 mm, which is shown in Figure 8(a); the plasma in the chamber is shown in Figure 8(b).

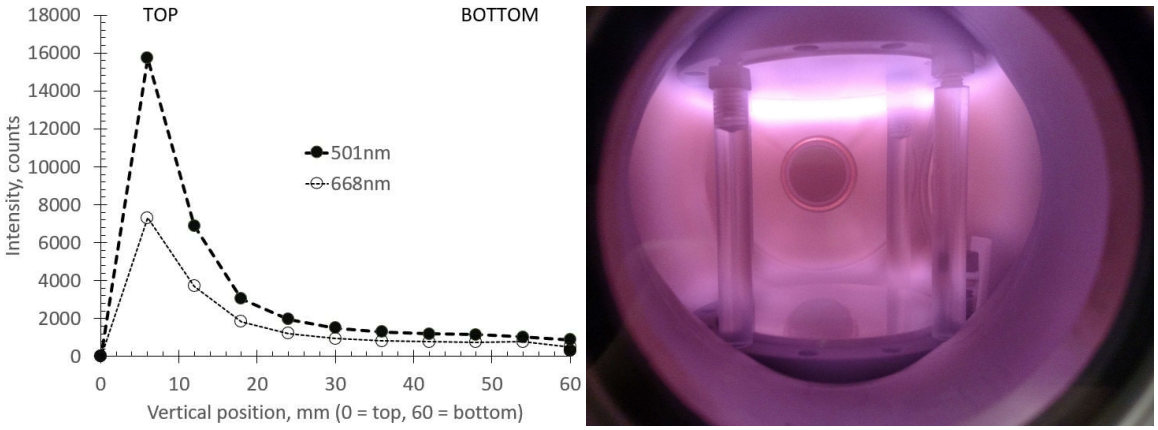

Figure 8: Plasma emission between the electrodes: (a) plotted emission intensity for 501nm, 668nm helium lines; (b) corresponding digital photograph of visible light output for the same plasma.

Because the lines are strongest closest to the top electrode (at left in the plot in Fig. 8(a)), the results support the idea that most of the RF energy is deposited near the top electrode. This idea is also borne out by visual inspection of the plasma in the chamber as in Fig. 8(b), since a brighter glowing area can be distinguished adjacent to the top electrode.

IV. Graphite-Triggered Laser Vaporization Test

This aspect of the experimental work did not produce the desired result; namely, deposition of laser energy directly into the plasma did not initiate a laser spark. However, in further review of the literature, it appears that this result is consistent with expectation since the threshold to ignite a plasma from the diffuse gas is significantly higher than our laser can produce. As an effort to bypass this difficulty, a graphite rod of 0.5 mm diameter was inserted into the experimental chamber so that its position coincided with the laser focus, with the idea that vaporization of the rod would lower the threshold to spark a plasma. Results from this test are displayed in Figure 9, including a high-speed image of the ablation event, and 2D and 3D diagrams of the optical profilometry of the aftermath.

Although material was certainly vaporized from the rod, the amount of material removed strongly suggests that our laser intensity is too low to generate strong shock waves. Theoretically, in order to

vaporize carbon, at least the bare minimum of energy must be supplied to heat the material to its vaporization point. In practice, for rapid surface heating, the latent heat of vaporization is generally much greater than the energy needed to heat or melt the material. Thus, the threshold laser energy per area for vaporization to occur can be estimated as:

$$F_{th} = 2L_v\sqrt{\frac{\rho\,\kappa\,\tau}{c}}\ , \qquad (4)$$

where L_v is the latent heat of vaporization (sublimation enthalpy), ρ is density, κ is the thermal conductivity, τ is laser pulse duration, and c is the specific heat of the material.[14]

(a) (b) (c)

Figure 9: Laser vaporization of carbon rod: (a) high-speed camera image of laser vaporizing carbon, (b) WLI optical profilometry 2D view, (c) WLI optical profilometry 3D view

For graphitic carbon, literature data with associated uncertainties [15(a),15(b),15(c),16] are shown in Table 4.

Table 4: Thermophysical Literature Data for Carbon

Parameter	T_v	ρ	κ	c	L_v
Units	K	kg/m^3	W/(m K)	J/(kg K)	J/kg
Value	3640 ± 25	2100 ± 200	140 ± 10	715 ± 4	(6.9 ± 0.2) × 10^7
Source	[15(a)]	[15(a)]	[15(b)]	[15(c)]	[16]

Based on the data in Table 4, the threshold would be predicted to lie around 2650 ± 230 J/cm^2, which is near the upper end of our presently achievable fluence using our laboratory's Nd:YAG laser focused to the smallest possible spot area, following equation (3) and accounting for reasonable beam losses before the beam reaches the target. Although limited vaporization of the graphite certainly is achievable, very little energy remains above that threshold to energize a plasma from the vapor, and so it is not surprising that no shock waves were observed. To overcome this obstacle, future experiments could make use of a different plasma seeding material with a much lower vaporization threshold, or use a laser with significantly higher pulse energy or significantly shorter laser pulse duration.

V. Future Work

Regarding future work, dust with a chemical composition similar to interstellar dust (e.g., coronene and silicon carbide) will be introduced into the plasma and a pulsed Nd:YAG laser will be used to spark a detonation. Shock wave pressure will be measured using a piezoelectric pressure sensor. A high-speed camera will record shock wave motion, at up to 200,000 frames per second, via schlieren imaging. The chemical composition and physical conformation of the dust particles will be measured before and after the test, using a scanning electron microscope, to determine if the explosion affected the size or composition of the particles.

Conclusions

This work reports the creation and initial testing of a radio frequency (RF) plasma chamber. A pair of aluminum electrodes were machined and connected to an RF source within a vacuum chamber to form capacitive RF plasmas. Spectroscopic data from 300-1000 nm, roughly consistent with literature spectra, were collected for argon and helium plasmas while the pressure of the chamber was varied from 5-270 Pa and power delivered to the plasma was varied from 1-100 W. Separately, the vertical position of the spectrometer was varied across the capacitive distance of 11 cm as a first step to collection information about the plasma temperature between the electrodes. Finally, a carbon rod was used in an unsuccessful attempt to initiate shock waves within the plasma.

Acknowledgments

This research was originally conceived by Dr. Elisha Polomski (College of San Mateo, San Mateo, CA). This study was supported by a Spring 2020 St. Cloud State University (SCSU) Student Research Award from Saint Cloud State University to Elatia Zaffke. The RF instrumentation was provided via a Fall 2016 SCSU Faculty Improvement Grant to Dr. Polomski. The 6” chamber was provided via SCSU research grants (Spring 2018 SCSU Early Career Award, and Fall 2017 SCSU Proposal Enhancement Grant) to Dr. Sinko.

The authors also thankfully acknowledge assistance from the SCSU College of Science and Engineering, the SCSU Department of Physics & Astronomy and its Office Administrative Specialist Denise Schaefer, and the SCSU Office of Research and Sponsored Programs staff, in particular Lorie Ortloff, Deb Rothstein, and Sheila Saiko. Significant assistance and time was also provided by Timothy Goodner and Dr. James Nicholson of the Department of Environmental and Technological Studies for metal machining of RF and vacuum components. Last but certainly not least, sincere thanks and acknowledgement for assistance in machining, fashioning and installation of electrodes and vacuum components for the RF chamber is extended to a participant from Iceland in the Summer 2019 Education USA Academy, Elísa Sverrisdòttir.

References

1. Dwek, E. & Arendt, R. G, 1992, Annual Review of Astronomy & Astrophysics 30, 11
2. Lewis, R., Anders, E. & Draine, B. Properties, detectability and origin of interstellar diamonds in meteorites. *Nature* **339,** 117–121 (1989).

3. P. O. Lagage, & C. J. Cesarsky, "The maximum energy of cosmic rays accelerated by supernova shocks," *Astronomy and Astrophysics*, *125*, 249-257, 1983.
4. H. T. Janka, & E. Mueller, "The first second of a Type II Supernova: Convection, accretion, and shock propagation," *The Astrophysical Journal Letters*, *448*(2), L109, 1995.
5. P. Chabert and N. Braithwaite, *Physics of Radio-Frequency Plasmas*, Cambridge University Press, New York, 2011, Ch. 5, pp. 131-175.
6. F. F. Chen, *Plasma Physics and Controlled Fusion*, Plenum Press, New York, 1984. (a) Ch. 1.4, pp. 10-11; (b) Ch. 5.1.1, p. 157.
7. A. Piel, *Plasma Physics*, Springer, New York, 2010, Ch. 4.2.1, p. 77.
8. S. T. Thornton and A. Rex, *Modern Physics for Scientists and Engineers*, *4th Ed.*, Cengage, Boston, 2013, Ch. 7, pp. 248-252.
9. A. Kramida, Yu. Ralchenko, J. Reader, and NIST ASD Team (2019). NIST Atomic Spectra Database (ver. 5.7.1), [Online]. Available: https://physics.nist.gov/asd [Accessed 4/15/2020]. National Institute of Standards and Technology, Gaithersburg, MD.
DOI: https://doi.org/10.18434/T4W30F
10. Murat Tanişli, İsmail Rafatov, Neslihan Şahin, Sercan Mertadam, and Süleyman Demira, "Spectroscopic study and numerical simulation of low-pressure radio-frequency capacitive discharge with argon downstream," *Canadian Journal of Physics*, Vol. 95, Issue 2, pp. 190-200, 2017.
11. David Mariotti, Yoshiki Shimizu, Takeshi Sasaki, and Naoto Koshizaki, "Method to determine argon metastable number density and plasma electron temperature from spectral emission originating from four 4p argon levels," Applied Physics Letters, Vol. 89, 201502, 2006.
12. Y.-G. Kang, H. Nishimura, H. Takabe, K. Nishihara, A. Sunahara, T. Norimatsu, K. Nagai, H. Kim, M. Nakatsuka, and H. J. Kong, "Laboratory Simulation of the Collision of Supernova 1987A with its Circumstellar Ring Nebula," *Plasma Physics Reports*, Vol. 27, Issue 10, pp. 843-851, 2001.
13. P. W. Milonni and J. H. Eberly, *Laser Physics*, John Wiley & Sons, Inc., Hoboken, 2010, Ch. 7.13, p. 320.
14. M. Stafe, A. Marcu, and N. N. Puscas, Pulsed Laser Ablation of Solids, Springer, New York, 2014.
15. *CRC Handbook of Chemistry and Physics*, 69th Ed., Eds. R. C. Weast, M. J. Astle, and W. H. Beyer, CRC Press, Boca Raton, 1988. (a) p. B-12 (b) p. E-12, (c) p. D-178.
16. P. D. Zavitsanos and G. A. Carlson, "Experimental Study of the Sublimation of Graphite at High Temperatures," *J. Chem. Phys.* **59**(6), pp. 2966-2973 (1973).